🄿 Selected for a Viewpoint in *Physics*

PHYSICAL REVIEW LETTERS

𝔖

Induced Charge Electro-osmosis over Controllably Contaminated Electrodes

Andrew J. Pascall and Todd M. Squires

Department of Chemical Engineering, University of California, Santa Barbara, California, USA
(Received 15 September 2009; published 22 February 2010)

Recent studies in nonlinear electrokinetics reveal the standard theory to generally overpredict measured velocities, sometimes dramatically. Contamination of the driving surface provides a natural mechanism for electrokinetic suppression. We measure induced charge electro-osmosis over gold electrodes "contaminated" with silica layers of controlled thickness for nearly a thousand distinct conditions, in a system that enables direct comparisons between theoretical predictions and experimental measurements. Both the magnitude and frequency dependence of the measured slip velocity are captured quantitatively over the entire range of experiments by accounting for the physical capacitance and surface chemistry of the dielectric layer. More generally, the quantitative characterization enabled by our apparatus will prove invaluable for the rational design and prediction of electrokinetic systems.

Electrokinetic (EK) effects involve the interaction between electric fields, electrolytic ions, fluid flows, and particle motion, and have a history dating back two centuries [1]. Recent years have seen a resurgence of interest in EK effects, including protein, DNA, and particulate separations, directed assembly of colloidal particles, and transport in micro- and nanofluidic devices [2].

Despite this long history and sustained interest, the most basic elements of electrokinetics have remained largely untested. The Helmholtz-Smoluchowski (HS) equation,

$$u_s = -\frac{\varepsilon_w \zeta_{eq} E}{\mu}, \tag{1}$$

relates the electro-osmotic flow (EOF) velocity u_s to the electrostatic potential drop ζ_{eq} across the diffuse layer of ions that screen a charged surface. Here ε_w and μ are the permittivity and viscosity of the electrolyte, respectively [Fig. 1(a)]. ζ_{eq} is difficult to manipulate experimentally, since it is generally set by surface chemistry [3], although some direct control has been shown in flow-FET systems [4]. While (1) is in principle predictive, its role in practice has most commonly been interpretive: given a measured u_s, (1) is used to infer ζ_{eq}. The design of complex microfluidic devices, however, will require reliable predictions for EK flows under a wide range of conditions.

A variety of nonlinear EK effects have been explored and exploited in recent years, including AC electrokinetic flows (ACEK) [5], electrokinetic instabilities [6], and induced charge electrokinetics (ICEK) [7–9]. All involve an applied field that perturbs the electrolyte (e.g., induces a charged double layer over a polarizable inducing surface), and then forces the perturbations into motion. An important advantage is that small AC potentials applied to closely spaced electrodes can produce large fields without electrolysis and drive steady nonlinear electrokinetic flows. Furthermore, the standard Poisson-Nernst-Planck (PNP) equations for ion transport make *quantitative* predictions for the steady flows driven by AC fields, which can be

directly compared against experimental measurements. Any discrepancies indicate physicochemical effects that are missing from the standard model.

While measured ICEK effects generally show qualitative agreement with theoretical predictions [8,10], both qualitative and quantitative discrepancies have been reported [9,11]. In particular, measured nonlinear electrokinetic flows in a variety of systems [11] are generally slower than the standard model predicts, sometimes by orders of magnitude. Various mechanisms have been proposed to explain this discrepancy, including Stern layers [12], steric interactions between double-layer ions [11,13] and noncontinuum effects.

Contamination of the inducing (metal) surface provides a natural mechanism for ICEK flow suppression [7]. To investigate this, we systematically contaminate inducing surfaces with silica (SiO_2) films of known thickness [$O(10 \text{ nm})$]. We compare measured ICEK flows against theory for 987 distinct experimental conditions, in which we vary electrolyte composition and concentration, electric
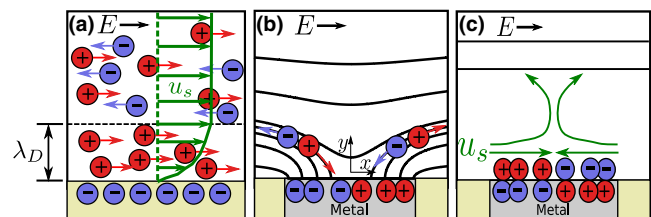

FIG. 1 (color online). (a) Electro-osmotic flow (EOF). A tangentially applied electric field forces the charged electric double-layer into motion. Outside the $\lambda_D \sim O(\text{nm})$ thick double-layer, the walls appear to "slip" with EOF velocity given by (1). (b)–(c) Induced charge electro-osmosis over an ideally polarizable metal strip. A suddenly applied electric field polarizes the metal strip, and (b) ions follow field lines to the metal surface. (c) Ions form a dipolar induced double layer (IDL) at steady state, leaving a tangential bulk electric field that drives the IDL into EOF.

field strength and frequency, and silica film thickness. In all cases, our system enables *quantitative* comparisons with the predictions of the PNP standard model. A naïve theory (computed as though no contaminant were present) fails in a manner reminiscent of many ICEK experiments [9,11]. Accounting for the physical capacitance of the dielectric and the "buffer capacitance" of known surface chemical reactions yields an unprecedented quantitative agreement between theory and experiment over the entire range of experiments.

We begin with the standard description of ICEK, in which an applied field *induces* a charged screening cloud around a polarizable surface, and then drives that *induced* cloud into electrokinetic motion. A suddenly applied electric field initially intersects *normal* to an (equipotential) metal strip [Fig. 1(b)], driving ions in solution toward the metal surface. In the absence of electrochemical (Faradaic) reactions, positive ions accumulate near the field source, and negative ions near the field sink, to form a dipolar induced double layer [Fig. 1(c)]. Steady state is achieved when the (capacitive) double layer is charged through the (resistive) electrolyte. This requires a characteristic RC charging time τ_c, after which the field $E_\parallel$ outside the double layer is purely tangent to the double layer. The induced zeta potential, $\zeta_i \sim E_\parallel x$, is the potential drop from the metal surface to the bulk electrolyte outside the double layer. The parallel field then forces the induced double layer to drive a nonlinear ICEK flow $u_s \sim E_\parallel^2 x$ [Fig. 1(c)]. Since reversing the field direction reverses the induced charge, a time-averaged ICEK flow is established even under AC fields, with frequency less than τ_c^{-1}.

In the quasisteady limit ($\omega \ll \tau_c^{-1}$), an applied field $E(t) = E_o \cos(\omega t)$ induces a quasisteady double layer with $\zeta_i = E(t)x$. Assuming ζ_i to superpose with the native ζ_{eq}, the time-averaged slip velocity is given by (1) to be

$$\frac{\mu \langle u_s \rangle}{\varepsilon_w} = -E_o \langle \cos\omega t (\zeta_{eq} + E_o x \cos\omega t) \rangle = -\frac{E_o^2 x}{2}. \quad (2)$$

Notably, ζ_{eq} does not survive the time average, and the quantitative prediction in (2) depends solely on variables that can be directly controlled in experiments.

Transient double-layer charging becomes important when $\omega \gtrsim \tau_c^{-1}$. In this system, as with ACEK over coplanar electrodes, the charging time scale depends upon the distance $|x|$ from the electrode's center line. Adapting the charging model in [5] leads to a time-averaged slip velocity that depends on both position and frequency:

$$\langle u_s \rangle = -\frac{\varepsilon_w E^2 x}{2\mu(1 + \tau_c^2 \omega^2)}, \quad (3)$$

where $\tau_c = \varepsilon_w (\pi |x|)/\sigma \lambda_D$, and σ is the electrolyte conductivity. Explicit numerical calculations (COMSOL AB) are in excellent agreement with (3).

We now describe our experiments [Fig. 2(a)]. We coated molecularly smooth fused silica plates (University Wafer) with a silane-thiol monolayer (as in [14], but with

575 mTorr O_2 plasma exposure) for adhesion. We patterned 50×900 μm electrodes by depositing 200 Å of gold at 0.5 Å/s via electron beam evaporation, then evaporated silica films of various thickness (33, 66, or 100 nm) on the same day, to prevent fouling of the electrode surface.

Using soft lithography [15], we microfabricated polydimethylsiloxane (PDMS) channels of length 1 cm, height 100 μm, and width 300 μm, which we ozone bonded to the substrate so that the microelectrode was located at the midpoint of the microchannel and oriented perpendicular to it [Fig. 2(a)]. We designed the electrode to minimize stray asymmetric flows due to capacitive coupling with the microscope [16]. Fluid ports were punched at the channel ends with 26 gauge Luer stubs (McMaster-Carr). Stainless steel pins (New England Small Tube, 23 gauge) were inserted to act as fluidic vias and driving electrodes.

Electrolytes of concentration 10, 1, 0.1, and 0.01 mM KCl or NaCl were made by diluting a 10 mM stock solution of the salt dissolved in Milli-Q water. 520 nm fluorescent microspheres (Bangs Laboratories, FS03F/5069) were added to each electrolyte (0.02 wt%) to serve as flow tracers for microparticle image velocimetry (μPIV).

Syringes were connected to the stainless steel pins via Tygon tubing, and an electrolyte of given ionic strength and composition (starting with the lowest ionic strength)
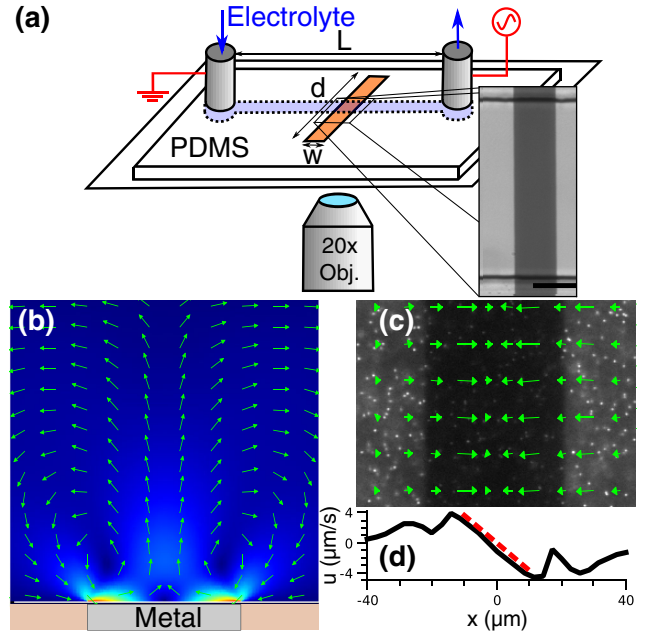

FIG. 2 (color online).   (a) A micropatterned gold electrode of width $w = 50$ μm and length $d = 900$ μm (inset, scale bar 50 μm), sits at the center of a PDMS microchannel of length $L = 1$ cm. Stainless steel tubes at the ends of the channel serve as both electrolyte ports and driving electrodes. (b) Computed ICEK flow, viewed along the electrode, shows two counterrotating cells. (c) A μPIV velocity field overlaid on an experimental image showing the flow-tracing microspheres. (d) The mean velocity profile from which the slope u' of the red dashed line is obtained.

was flowed into the channel. Electric leads were attached to the stainless steel pins and driven with a sinusoidal potential (Agilent 33220A function generator, amplified by a Trek PZD350 M/S). For each electrode-electrolyte combination, an automated system (Labview, National Instruments) applied AC potentials from 50–150 V to the stainless steel pins at frequencies from 100 Hz–30 kHz. Between runs, the channel was flushed with at least 1 ml of the next electrolyte. Fluorescence video microscopy (Andor iXon 885, Nikon TE2000-U with 20× ELWD, 0.45 NA objective) was used to record microsphere positions and μPIV algorithms were used to determine velocity profiles [Fig. 2(c)], which were corrected for the finite depth of focus of the optics [17]. A detailed description of similar experimental protocols is given in [16].

We average along the electrode to obtain the mean velocity profile [Fig. 2(d)]. The slope u' of this profile over the central 20 μm of the electrode was recorded [18]. 987 trials had a velocity above the error threshold (set so that Brownian motion of the tracer particles accounts for less than 20% of the observed velocity [17]).

Figure 3(a) shows measured slip velocities u', scaled by $u'_o = -\varepsilon_w E^2/2\mu$ from the naïve ICEK theory (as if the metal were clean), plotted versus frequency (scaled by $\tau_c = \varepsilon_w(\pi|x_e|)/\sigma\lambda_D$, with $|x_e| = 10$ μm at the edge of the region of interest). Measured velocities at low frequencies ($\tau_c\omega \ll 1$) are 10–1000 times slower than predicted by theory, and the frequency dependence is poorly captured by the theory.

Of course, the naïve theory omits the silica contaminant, which splits the total potential drop, $\Delta V = Ex$, between the double-layer $\zeta_i = Ex/(1 + \delta)$, which contributes to ICEK flow, and the dielectric $\Delta V_d = \delta Ex/(1 + \delta)$, which does not [7]. Here $\delta = \varepsilon_w d/\varepsilon_d\lambda_D$ is the ratio of linearized double layer to dielectric layer capacitances, where $\varepsilon_d = 4.6$ and d are the permittivity and thickness of the silica layer. Here, δ ranged from 0.18–566. The dielectric reduces both u_s and τ_c:

$$u'_{\text{phys}} = u'_o(1 + \delta)^{-1}, \qquad \tau_{\text{phys}} = \tau_c(1 + \delta)^{-1}. \quad (4)$$

Scaling the measured velocities to account for the physical dielectric improves agreement [Fig. 3(b)], yet significant scatter remains even between experiments with the same d. The nonlinear double-layer capacitance, $C_{\text{DL}} = \varepsilon_w/\lambda_D \cosh(e\zeta/2k_BT)$, here leads to at most 20% changes, which is insufficient to account for these discrepancies. A missing mechanism thus remains.

Silica surfaces contain silanol groups which can react with hydronium (H$^+$) ions in the double layer via

$$\text{SiOH} \rightleftharpoons \text{SiO}^- + \text{H}^+, \quad (5)$$
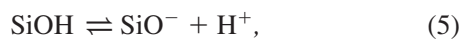
which we assume to be in quasiequilibrium with the hydronium ion concentration in the double layer. An increase (decrease) in ζ_i lowers (raises) $[\text{H}^+]_s$ in the double layer, which shifts the equilibrium in (5) to the left (right). The surface "buffers" changes in $[\text{H}^+]_s$, introducing a buffer

capacitance in parallel with the double layer [19]:

$$C_{\text{buff}} = \frac{e^2 N_s}{k_B T}\left(\frac{K_a a_\text{H}\exp(-e\zeta/k_BT)}{[K_a + a_\text{H}\exp(-e\zeta/k_BT)]^2}\right), \quad (6)$$

where N_s is the silanol site density, $K_a \sim 10^{-6}$ is the equilibrium constant for (5), and a_H is the activity of H$^+$ in the bulk electrolyte. A related model for ion adsorption [20] was found to better fit ACEK measurements [12].

Accounting for both buffer and physical capacitances yields $\zeta_i = Ex/(1 + \delta + \beta)$, where $\beta = C_{\text{buff}}/C_d$. The theoretical slip velocity and RC time become
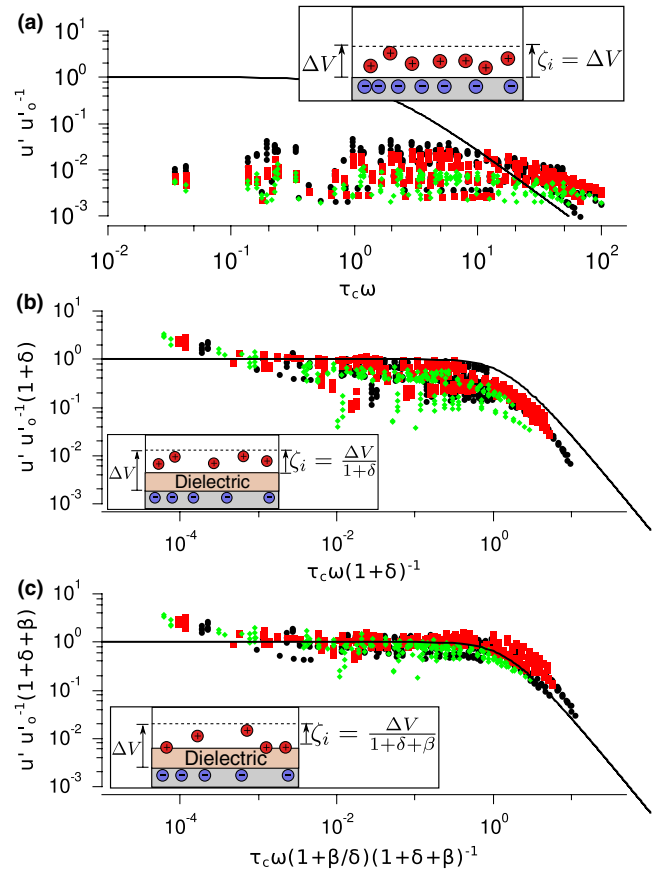

FIG. 3 (color online). Normalized slip velocity vs dimensionless frequency. Data points are coded by silica film thickness: ($\bullet$, black) 33 nm, ($\blacksquare$, red) 66 nm, ($\blacklozenge$, green) 100 nm. Solid lines represent theoretical predictions. (a) u' scaled by the naïve ICEK theory, ignoring the dielectric. Inset: Neglecting the dielectric layer, all of the potential difference ΔV between the electrode and the bulk electrolyte occurs over the double layer. (b) u' scaled assuming the dielectric acts only as a physical capacitor, in series with the double layer. Inset: The physical capacitance of the dielectric layer reduces ζ_i by $(1 + \delta)^{-1}$, where $\delta = C_{\text{DL}}/C_d$. (c) u' scaled accounting for both surface chemistry (via buffer capacitance C_{buff}) and the physical capacitance. Inset: Surface chemistry immobilizes some ions that would otherwise contribute to EK flows, further reducing $\zeta_i = \Delta V/(1 + \delta + \beta)$, where $\beta = C_{\text{buff}}/C_d$. 99% of all measurements (representing 987 distinct conditions) lie within a factor of 3 of this theory.

$$u'_{\text{BP}} = \frac{u'_o}{1 + \delta + \beta}, \qquad \tau_{\text{BP}} = \frac{1 + \beta/\delta}{1 + \delta + \beta}\tau_c. \qquad (7)$$

Here N_s, a_{H}, and ζ_{eq} are specific to the experimental system and are required to calculate C_{buff}. Reasonable bounds are known: $N_s \leq 7.8 \text{ nm}^{-2}$ and $-50 \leq \zeta_{\text{eq}} \leq -25 \text{ mV}$ [3]. The in-channel pH of the electrolyte was determined to be ≤ 4 via fluorescent indicators.

Since ζ_i is generally low in our experiments (0.2–10.3 mV), and N_s and ζ_{eq} do not vary significantly between experiments, a single value for C_{buff} is expected for all experiments. Indeed, setting $C_{\text{buff}} = 24 \text{ mF m}^{-2}$ yields remarkable agreement, capturing both the magnitude and frequency dependence of the theory for 987 experiments [Fig. 3(c)]. 99% of the data lie within a factor of 3 of theory. Additionally, the above parameter bounds yield a consistent magnitude for C_{buff}. By contrast, poor fits are obtained using a linear Stern layer (in series with the double layer and dielectric) instead of C_{buff}.

A curious trend appears at low frequencies [Fig. 3(c)], in which theory *underpredicts* measurements, for the highest salt concentrations (10 mM KCl and NaCl). While the cause is unknown, the high mobility of H$^+$ (which sets C_{buff}) relative to salt ions (which do not) may play a role.

Induced zeta potentials in these experiments were relatively small ($\zeta_i < k_B T/e$), and well described by the linear theory. A variety of interesting effects (e.g., nonlinear capacitance, modified charging dynamics, ion crowding, and flow reversal) arise in the nonlinear regime ($\zeta_i > k_B T/e$) [5,11,13]. Our system enables a continuous transition between linear and nonlinear systems, and an important future direction will be to interrogate nonlinear induced double layers.

To summarize, we have demonstrated an unprecedented agreement between theoretical predictions and experimental measurements of ICEK flow over controllably contaminated surfaces. Values from nearly a thousand distinct experiments, representing a wide range of conditions, collapse onto a single theoretical curve that accounts for the physical dielectric contaminant and its surface chemistry.

Of course, understanding how contaminants reduce ICEK velocities does not mitigate this velocity reduction. Having elucidated these mechanisms, however, we can suggest strategies to maximize ICEK more generally by using thin surface coatings (to minimize C_d) and low ion reactivity (to minimize C_{buff}). Our experimental system is remarkably general, and enables the rapid EK characterization of *any* material that can be deposited as a thin film atop a planar electrode, under a range of conditions and electrolytes. High-throughput searches to optimize materials for ICEK systems are thus within reach.

[1] F. F. Reuss, Mem. Soc. Imp. Nat. Moscou **2**, 327 (1809).
[2] T. M. Squires and S. R. Quake, Rev. Mod. Phys. **77**, 977 (2005); R. B. Schoch and P. Renaud, Rev. Mod. Phys. **80**, 839 (2008).
[3] B. J. Kirby and E. F. Hasselbrink, Electrophoresis **25**, 187 (2004).
[4] R. B. M. Schasfoort, S. Schlautmann, L. Hendrikse, and A. van den Berg, Science **286**, 942 (1999).
[5] A. Ramos, H. Morgan, N. G. Green, and A. Castellanos, J. Colloid Interface Sci. **217**, 420 (1999); A. Ajdari, Phys. Rev. E **61**, R45 (2000); A. Ramos, H. Morgan, N. G. Green, A. Gonzalez, and A. Castellanos, J. Appl. Phys. **97**, 084906 (2005).
[6] J. D. Posner and J. G. Santiago, J. Fluid Mech. **555**, 1 (2006); G. Yossifon and H. C. Chang, Phys. Rev. Lett. **101**, 254501 (2008).
[7] T. M. Squires and M. Z. Bazant, J. Fluid Mech. **509**, 217 (2004).
[8] C. K. Harnett, J. Templeton, K. A. Dunphy-Guzman, Y. M. Senousy, and M. P. Kanouff, Lab Chip **8**, 565 (2008).
[9] T. M. Squires, Lab Chip **9**, 2477 (2009).
[10] S. Gangwal, O. J. Cayre, M. Z. Bazant, and O. D. Velev, Phys. Rev. Lett. **100**, 058302 (2008); J. A. Levitan, S. Devasenathipathy, V. Studer, Y. X. Ben, T. Thorsen, T. M. Squires, and M. Z. Bazant, Colloid Surf. A **267**, 122 (2005); A. B. D. Brown, C. G. Smith, and A. R. Rennie, Phys. Rev. E **63**, 016305 (2000); J. P. Urbanski, T. Thorsen, J. A. Levitan, and M. Z. Bazant, Appl. Phys. Lett. **89**, 143508 (2006).
[11] M. Z. Bazant, M. S. Kilic, B. D. Storey, and A. Ajdari, Adv. Colloid Interface Sci. **152**, 48 (2009); M. Z. Bazant, M. S. Kilic, B. D. Storey, and A. Ajdari, New J. Phys. **11**, 075016 (2009).
[12] N. G. Green, A. Ramos, A. Gonzalez, H. Morgan, and A. Castellanos, Phys. Rev. E **66**, 026305 (2002).
[13] B. D. Storey, L. R. Edwards, M. S. Kilic, and M. Z. Bazant, Phys. Rev. E **77**, 036317 (2008).
[14] A. K. Mahapatro, A. Scott, A. Manning, and D. B. Janes, Appl. Phys. Lett. **88**, 151917 (2006).
[15] D. C. Duffy, J. C. McDonald, O. J. A. Schueller, and G. M. Whitesides, Anal. Chem. **70**, 4974 (1998).
[16] T. S. Mansuripur, A. J. Pascall, and T. M. Squires, New J. Phys. **11**, 075030 (2009).
[17] S. T. Wereley and C. D. Meinhart, Annu. Rev. Fluid Mech. **42**, 557 (2010).
[18] See supplementary material at http://link.aps.org/supplemental/10.1103/PhysRevLett.104.088301 for the complete data set.
[19] R. E. G. van Hal, J. C. T. Eijkel, and P. Bergveld, Adv. Colloid Interface Sci. **69**, 31 (1996); E. J. van der Wouden, D. C. Hermes, J. G. E. Gardeniers, and A. Berg, Lab Chip **6**, 1300 (2006).
[20] Y. K. Suh and S. Kang, Phys. Rev. E **79**, 046309 (2009).